中國機械工程學刊第四十五卷第六期第 517~531 頁(民國一百一十三年)
Journal of the Chinese Society of Mechanical Engineers, Vol.45, No.6, pp517~531 (2024)

Generation, Modeling, and Analysis of Curvilinear Cylindrical Gear Drive Featuring Predesigned Fourth-Order Transmission Error and Cosine Tooth Profile

Cheng-Kang Lee* and Yung-Chang Cheng**

Keywords： curvilinear cylindrical gear, cosine tooth profile, fourth-order transmission error, CAD/CAM, four-axis computer numerical control (CNC) machining.

ABSTRACT

This study proposes an innovative curvilinear cylindrical gear drive characterized by a predesigned fourth-order transmission error and a cosine tooth profile. The predesigned fourth-order transmission error not only absorbs linear transmission errors but also contributes to a smoother overall motion curve. The cosine tooth profile helps reduce the minimum number of teeth without undercutting. This research begins by establishing the generation methods and mathematical models for both the curvilinear pinion and gear. A set of nonlinear simultaneous equations, consisting of fifteen unknowns and fifteen equations, is then formulated based on tooth contact conditions and the predesigned fourth-order transmission error condition. The differential evolution algorithm and Newton's method are subsequently employed to conduct a global search and local refinement of the unknowns, leading to precise design solutions for the generating motion parameters. Tooth Contact Analysis (TCA) theory is applied to verify that the actual transmission error aligns perfectly with the predesigned fourth-order transmission error and to confirm that the contact ellipses and bearing contacts are centrally located on the tooth surface. Finally, to further validate the theoretical accuracy, CAD/CAM technology and a four-axis computer numerical control (CNC) machine are used to fabricate a curvilinear cylindrical gear drive. After inspecting the bearing contact positions using red ink, it is confirmed that the actual contact situation corresponds with the theoretical results.

Paper Received June, 2024. Revised September, 2024. Accepted October, 2024. Author for Correspondence: Cheng-Kang Lee.

* *Professor, Department of Industrial Engineering and Management, Cheng Shiu University, Kaohsiung, Taiwan 833301, ROC.*

** *Professor, Department of Mechatronics Engineering, National Kaohsiung University of Science and Technology, Kaohsiung, Taiwan 824005, ROC.*

INTRODUCTION

Curvilinear cylindrical gears are cylindrical gears with arcuate tooth traces, featuring convex arcuate tooth traces on one side of the tooth surface and concave arcuate tooth traces on the other. Koga's patent (1975) introduced a method for cutting paired gears with arcuate tooth traces, employing face milling cutters with male and female cutting blades for simultaneous and precise tooth thread formation. Liu (1988) explored the historical and practical aspects of curvilinear cylindrical gears, tracing their ancient origins to the Warring States period and detailing successful modern production since 1980, overcoming technical challenges with specialized machinery. Tseng and Tsay (2001) laid the foundation for understanding cylindrical gears with curvilinear-shaped teeth, employing a mathematical model and rack cutter methodology grounded in gearing theory, facilitating profile generation, and providing crucial insights into tooth undercutting for field advancements. Tseng and Tsay (2004) investigated the contact characteristics of cylindrical gears with curvilinear-shaped teeth, revealing minimal transmission errors and concentrated bearing contacts in the central region of the gear pair, even under axial misalignments. Arafa (2005) explored cylindrical gears with lengthwise curved teeth, known as C-gears, highlighting their geometrical features, cutting methods, and potential applications. Tseng and Tsay (2005) proposed a mathematical model for cylindrical gears with curvilinear-shaped teeth cut by a CNC hobbing machine, investigating tooth surface deviations and offering insights into the manufacturing process. Tseng and Tsay (2006) explored the undercutting and contact characteristics of cylindrical gears with curvilinear-shaped teeth generated by hobbing, analyzing kinematic errors and contact ellipses under different assembly conditions and design parameters. Wu et al. (2009) proposed circular-arc curvilinear tooth gear drives, analyzing kinematical errors and contact patterns using complemented circular-arc rack cutters with curvilinear tooth traces, providing insights into the system's behavior under different assembly conditions. Chen and Gu (2011) examined a modified curvilinear gear set, revealing continuous transmission errors and localized bearing contact, with insights into the impacts of assembly errors and design parameters on contact characteristics. Fuentes et al. (2014) proposed two circular-arc curvilinear-shaped teeth gear geometries generated by face-milling cutters, employing computerized processes to simulate meshing, tooth contact analysis, and finite element analysis and revealing the advantages and disadvantages of the designs. Zhang et al. (2016) proposed a unique method for processing curvilinear tooth gears with a single blade cutter, examining meshing and contact characteristics and demonstrating potential advantages, including a higher contact ratio and suitability to replace spur gears in specific applications. Chen and Lo (2015) conducted a comprehensive study employing finite element analysis to investigate the loaded tooth contact analysis, contact stress, and transmission errors of a modified curvilinear gear set with localized bearing contact, providing valuable insights into the performance under different design parameters and loads. Chen et al. (2017) aimed to enhance the meshing characteristics of a complementary curvilinear gear set generated by complementary rack cutters, utilizing mathematical modeling, tooth contact analysis (TCA), and finite element analysis (FEA) to improve contact patterns, reduce sensitivity to assembly errors, and calculate contact stress. Zhang and Liang (2021) conducted a comprehensive study on curvilinear cylindrical gears with line contact, employing fixed-setting face-milling cutters and addressing mathematical modeling, tooth contact analysis, and stress analysis, highlighting insights into ideal and error conditions, as well as the effectiveness of tip relief in mitigating contact stresses. Wei et al. (2022) explored the contact characteristics of variable hyperbolic circular-arc-tooth-trace (VH-CATT) cylindrical gears, establishing a tooth surface contact analysis (TCA) model that considered installation errors and analyzed the influence of different errors and design parameters on geometric contact characteristics and sensitivity of the gear pair. Wu et al. (2023) conducted a thorough analysis of loaded meshing characteristics in cylindrical gear transmission with curvilinear-shaped teeth, providing insights into contact distribution, stress, load, and transmission errors, along with discussions on the impact of design parameters, serving as a theoretical tool for related analyses and modifications.

Gear drives are essential components in power transmission systems, serving a diverse range of applications. Transmission errors and localized bearing contact play pivotal roles in shaping the design and performance of gears, influencing factors such as noise, vibrations, and overall efficiency. Numerous studies have been undertaken to comprehend and manage these phenomena, particularly in gears featuring modified geometries. Several investigations have been conducted on spur, helical, worm, bevel, and face gears. Litvin et al. (1988) proposed modifications to tooth surfaces, introducing parabolic transmission errors to address linear transmission errors arising from misalignments and to obtain localized bearing contact. Litvin and Lu (1995) performed computerized simulations for double circular-arc helical gears, investigating the influence of gear misalignment on transmission errors and demonstrating the practical application of modified geometries through numerical examples. Seol and Litvin (1996) concentrated on worm-gear drives, suggesting the application of computerized methods to simulate meshing and contact in misaligned drives, along with proposing geometry modifications for localized and stabilized bearing contact. Litvin and Kim (1997) introduced modifications to spur gear geometry, with the goal of achieving localized bearing contact and reduced transmission errors, showcasing the advantages through computer programs and numerical examples. De Donno and Litvin (1999) introduced a novel approach for designing low-noise worm gear drives with stable bearing contact, confirming the effectiveness of the proposed oversized hob and varied plunging of worm-gear generating tools through computerized simulation. Litvin et al. (2000) explored face worm-gear drives with methods for localizing bearing contact and reducing transmission errors, demonstrating the benefits of this approach through double-crowning of the worm and a dedicated computer program for simulation. Stadtfeld and Gaiser (2000) introduced the ultimate motion graph concept, which was employed to modulate tooth surfaces and reduce gear noise in bevel and hypoid gear drives. Lee and Chen (2004) proposed mathematical models for cylindrical gear sets with parabolic cutting edges, emphasizing their improved robustness against assembly errors due to localized bearing contact. Wang and Fong (2006) focused on fourth-order kinematic synthesis for face-milling spiral bevel gears, achieving a notable reduction in loaded transmission error through numerical simulations. Lee (2009) presented a manufacturing process for a cylindrical crown gear drive with a controllable fourth-order polynomial function of transmission error, and the design's effectiveness in reducing gear running noise was validated through mathematical models and simulations. Jiang and Fang (2015) designed and analyzed modified cylindrical gears with controllable higher-order transmission error using particle swarm optimization, demonstrating through numerical simulations a lower amplitude of loaded transmission error. Lee (2018) proposed a method for designing a face gear drive with a predesigned fourth-order function of transmission errors, aiming to reduce noise and vibration. Lee (2019) introduced the cosine face gear drive, which features a predesigned fourth-order function of transmission errors and effectively overcomes traditional undercutting issues.

This study presents an innovative application of a predesigned fourth-order transmission error and a cosine tooth profile to a novel curvilinear cylindrical gear drive. The paper includes the following tasks: (i) developing the generation method for the drive, (ii) establishing the mathematical model for tooth surfaces, (iii) formulating a system of constrained equations to introduce the predesigned fourth-order transmission error, (iv) executing the differential evolution algorithm and Newton's root-finding method to determine the design values for the undetermined generating motion parameters, (v) conducting tooth contact analysis to validate real transmission error, (vi) using Recurdyn to simulate meshing and contact pressure, (vii) employing Siemens NX to generate machining programs, (viii) simulating the machining process using VERICUT and verifying the correctness of the program, (ix) machining the gear drive using a real four-axis CNC machine tool, and (x) inspecting the bearing contacts of the gear drive using red ink.

GENERATION METHOD AND MATHEMATICAL MODEL

As illustrated in Fig. 1, the novel curvilinear cylindrical gear drive consists of a pinion and a gear, represented by symbols 1, 11, and 12 for the gear drive, pinion, and gear, respectively.

The Generation Method and Mathematical Model of the Pinion

As shown in Fig. 2, pinion 11 is generated by the revolution surface, denoted by 111, which can be formed by either a cutting edge or a grinding wheel. As shown in Fig. 3, the axial section shape of the revolution surface 111 is a curve defined using a cosine function, denoted by 1111. The revolution axis of the revolution surface 111 is A_1. The radius parameter of the revolution surface 111 is ρ_1. Let the coordinate system $S_1(x_1, y_1, z_1)$ be rigidly connected to the axial section profile 1111. The position vector function of the axial section profile 1111 can be represented in $S_1(x_1, y_1, z_1)$ by $\mathbf{r}_1(u_1)$.

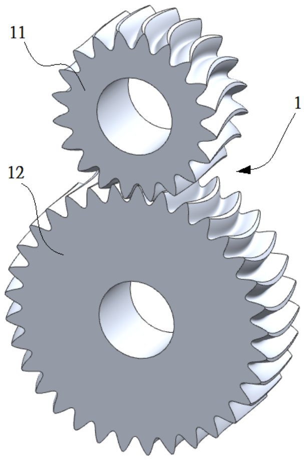

Fig. 1 The novel curvilinear cylindrical gear drive.

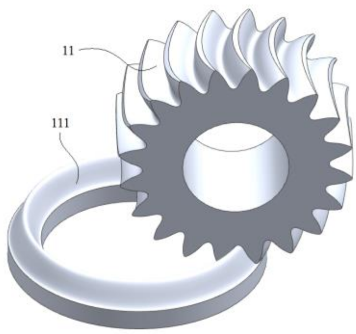

Fig. 2 Pinion 11 and revolution surface 111.

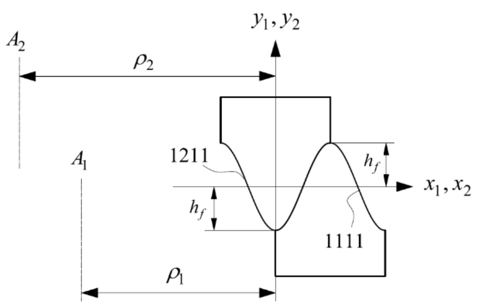

Fig. 3 Profiles 1111 and 1211 are cosine function curves.

$$\mathbf{r}_1(u_1) = \begin{bmatrix} x_1 \\ y_1 \\ z_1 \end{bmatrix} = \begin{bmatrix} u_1 \\ -h_f \cos(2u_1/m) \\ 0 \end{bmatrix} \quad (1)$$

To create the position vector function of the revolution surface 111, let the coordinate system $S_3(x_3, y_3, z_3)$ be rigidly connected to the revolution surface 111. The relationship between coordinate systems $S_1(x_1, y_1, z_1)$ and $S_3(x_3, y_3, z_3)$ is shown in Fig. 4.

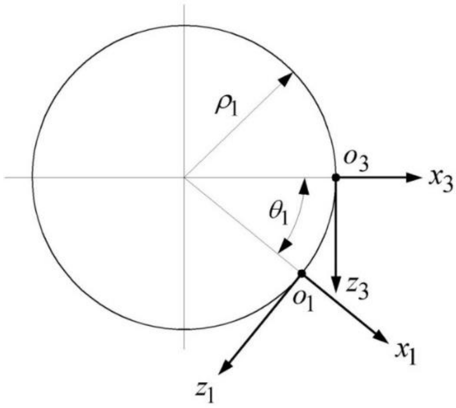

Fig. 4 Relationship between $S_1(x_1, y_1, z_1)$ and $S_3(x_3, y_3, z_3)$.

In $S_3(x_3, y_3, z_3)$, the position vector function of the revolution surface 111 is $\mathbf{r}_3(u_1, \theta_1)$.

$$\mathbf{r}_3(u_1,\theta_1)=\begin{bmatrix} -\rho_1+(u_1+\rho_1)\cos\theta_1 \\ -h_f\cos(2u_1/m) \\ (u_1+\rho_1)\sin\theta_1 \end{bmatrix} \tag{2}$$

In $S_3(x_3, y_3, z_3)$, the normal vector function of the revolution surface 111 is $\mathbf{N}_3(u_1, \theta_1)$, and the unit normal vector function is $\mathbf{n}_3(u_1, \theta_1)$.

$$\mathbf{N}_3(u_1,\theta_1)=\frac{\partial\mathbf{r}_3(u_1,\theta_1)}{\partial\theta_1}\times\frac{\partial\mathbf{r}_3(u_1,\theta_1)}{\partial u_1} \tag{3}$$

$$\mathbf{n}_3(u_1,\theta_1)=\mathbf{N}_3(u_1,\theta_1)/\left|\mathbf{N}_3(u_1,\theta_1)\right| \tag{4}$$

Let the coordinate system $S_p(x_p, y_p, z_p)$ be rigidly connected to the pinion 11. When the revolution surface 111 generates the pinion 11, the relative motion relationship between $S_3(x_3, y_3, z_3)$ and $S_p(x_p, y_p, z_p)$ is shown in Fig. 5. The coordinate system $S_3(x_3, y_3, z_3)$ undergoes a linear translation along the $(-x_3)$ direction with the parameter s_p , and the coordinate system $S_p(x_p, y_p, z_p)$ rotates counterclockwise about the z_p axis with the parameter ϕ_p . The relationship between the parameters s_p and ϕ_p can be expressed as a fourth-order polynomial function $s_p(\phi_p)$.

$$\begin{aligned} s_p(\phi_p) &= \rho_p\phi_p + C_2{\phi_p}^2 + C_3{\phi_p}^3 + C_4{\phi_p}^4 \\ &= (mT_p/2)\phi_p + C_2{\phi_p}^2 + C_3{\phi_p}^3 + C_4{\phi_p}^4 \end{aligned} \tag{5}$$

where m is the module, T_p is the number of teeth of the pinion 11, and C_2 , C_3 , and C_4 are the undetermined coefficients for generating the predesigned fourth-order transmission error.

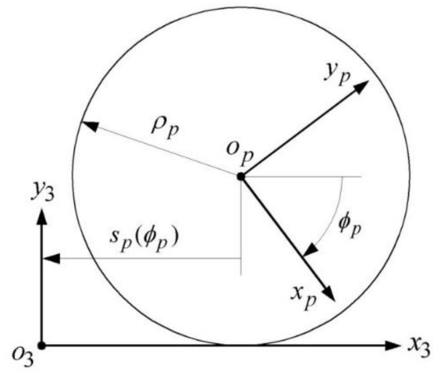

Fig. 5 Relationship between $S_3(x_3, y_3, z_3)$ and $S_p(x_p, y_p, z_p)$.

In the coordinate system $S_p(x_p, y_p, z_p)$, the revolution surface 111 forms a family of surfaces $\{\Sigma_p\}$, the position vector function of which is $\mathbf{r}_p^{(3)}(u_1, \theta_1, \phi_p)$.

$$\mathbf{r}_p^{(3)}(u_1,\theta_1,\phi_p)=\mathbf{M}_{p3}(\phi_p)\mathbf{r}_3(u_1,\theta_1) \tag{6}$$

where

$$\mathbf{M}_{p3}(\phi_p) = \begin{bmatrix} \cos\phi_p & -\sin\phi_p & 0 & -s_p(\phi_p)\cos\phi_p+\rho_p\sin\phi_p \\ \sin\phi_p & \cos\phi_p & 0 & -s_p(\phi_p)\sin\phi_p-\rho_p\cos\phi_p \\ 0 & 0 & 1 & 0 \\ 0 & 0 & 0 & 1 \end{bmatrix}$$

The unit normal vector function of the family of surfaces $\{\Sigma_p\}$ is $\mathbf{n}_p^{(3)}(u_1, \theta_1, \phi_p)$.

$$\mathbf{n}_p^{(3)}(u_1,\theta_1,\phi_p)=\mathbf{L}_{p3}(\phi_p)\mathbf{n}_3(u_1,\theta_1) \tag{7}$$

where

$$\mathbf{L}_{p3}(\phi_p)=\begin{bmatrix}\cos\phi_p & -\sin\phi_p & 0\\ \sin\phi_p & \cos\phi_p & 0\\ 0 & 0 & 1\end{bmatrix}$$

The necessary condition for the existence of the envelope of the family of surfaces $\{\Sigma_p\}$ is as follows:

$$\begin{cases} f_1(u_1,\theta_1,\phi_p)=\mathbf{n}_3(u_1,\theta_1)\cdot\mathbf{V}_3^{(3p)}(u_1,\phi_p)=0\\ \mathbf{V}_3^{(3p)}(u_1,\phi_p)=\begin{bmatrix}-y_1+\rho_p-s'_p(\phi_p)\\ -s_p(\phi_p)-\rho_1+(x_1+\rho_1)\cos\theta_1\\ 0\end{bmatrix}\end{cases} \tag{8}$$

The position vector function of the pinion 11 can be mathematically represented as

$$\begin{cases}\mathbf{r}_p(u_1,\theta_1,\phi_p)=\mathbf{r}_p^{(3)}(u_1,\theta_1,\phi_p)\\ f_1(u_1,\theta_1,\phi_p)=\mathbf{n}_3(u_1,\theta_1)\cdot\mathbf{V}_3^{(3p)}(u_1,\phi_p)=0\end{cases} \tag{9}$$

The unit normal vector function of the pinion 11 can be mathematically represented as

$$\begin{cases}\mathbf{n}_p(u_1,\theta_1,\phi_p)=\mathbf{n}_p^{(3)}(u_1,\theta_1,\phi_p)\\ f_1(u_1,\theta_1,\phi_p)=\mathbf{n}_3(u_1,\theta_1)\cdot\mathbf{V}_3^{(3p)}(u_1,\phi_p)=0\end{cases} \tag{10}$$

The Generation Method and Mathematical Model of the Gear

As shown in Fig. 6, gear 12 is generated by the revolution surface, denoted by 121, which can be created by either a cutting edge or a grinding wheel.

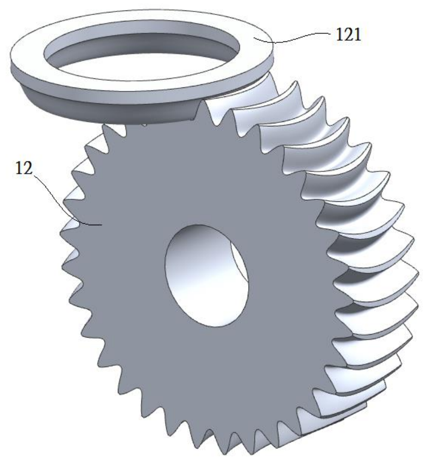

Fig. 6 Gear 12 and revolution surface 121.

As shown in Fig. 3, the axial section shape of the revolution surface 121 is the cosine function curve, denoted by 1211. The revolution axis of the revolution surface 121 is A_2. The radius parameter of the revolution surface 121 is ρ_2. Let the coordinate system $S_2(x_2,y_2,z_2)$ be rigidly connected to the axial section profile 1211, then the position vector function of the axial section profile 1211 can be represented in $S_2(x_2,y_2,z_2)$ by $\mathbf{r}_2(u_2)$.

$$\mathbf{r}_2(u_2)=\begin{bmatrix}x_2\\ y_2\\ z_2\end{bmatrix}=\begin{bmatrix}u_2\\ -h_f\cos(2u_2/m)\\ 0\end{bmatrix}, \tag{11}$$
$$-\pi m/2\le u_2\le \pi m/2$$

To create the position vector function of the revolution surface 121, let the coordinate system $S_4(x_4,y_4,z_4)$ be rigidly connected to the revolution surface 121. The relationship between coordinate systems $S_2(x_2,y_2,z_2)$ and $S_4(x_4,y_4,z_4)$ is shown in Fig. 7.

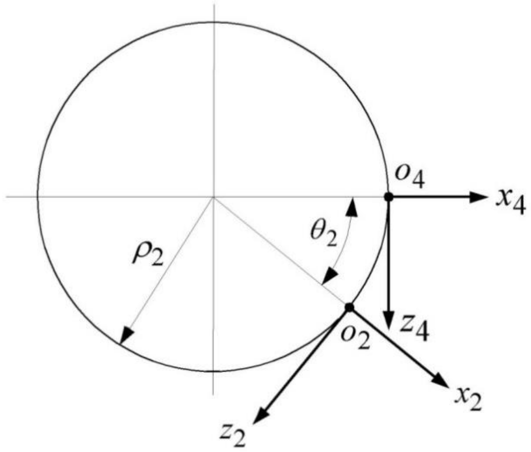

Fig. 7 Relationship between $S_2(x_2,y_2,z_2)$ and $S_4(x_4,y_4,z_4)$.

In $S_4(x_4,y_4,z_4)$, the position vector function of the revolution surface 121 is $\mathbf{r}_4(u_2,\theta_2)$.

$$\mathbf{r}_4(u_2,\theta_2)=\begin{bmatrix}-\rho_2+(u_2+\rho_2)\cos\theta_2\\ -h_f\cos(2u_2/m)\\ (u_2+\rho_2)\sin\theta_2\end{bmatrix} \tag{12}$$

In $S_4(x_4,y_4,z_4)$, the normal vector function of the revolution surface 121 is $\mathbf{N}_4(u_2,\theta_2)$, and the unit normal vector function is $\mathbf{n}_4(u_2,\theta_2)$.

$$\mathbf{N}_4(u_2,\theta_2)=\frac{\partial\mathbf{r}_4(u_2,\theta_2)}{\partial\theta_2}\times\frac{\partial\mathbf{r}_4(u_2,\theta_2)}{\partial u_2} \tag{13}$$

$$\mathbf{n}_4(u_2,\theta_2)=\mathbf{N}_4(u_2,\theta_2)/\left|\mathbf{N}_4(u_2,\theta_2)\right| \tag{14}$$

Let the coordinate system $S_g(x_g,y_g,z_g)$ be rigidly connected to the gear 12. When the revolution surface 121 generates the gear 12, the relative motion relationship between $S_4(x_4,y_4,z_4)$ and $S_g(x_g,y_g,z_g)$ is shown in Fig. 8. The coordinate system $S_4(x_4,y_4,z_4)$ undergoes a linear translation along the $(-x_4)$ direction with the parameter s_g, and the coordinate system $S_g(x_g,y_g,z_g)$ rotates about the z_g axis with the parameter ϕ_g. The relationship between the parameters s_g and ϕ_g is a first-order polynomial function $s_g(\phi_g)$.

$$s_g(\phi_g)=\rho_g\phi_g=(mT_g/2)\phi_g \tag{15}$$

where m is the module and T_g is the number of teeth of the gear 12.

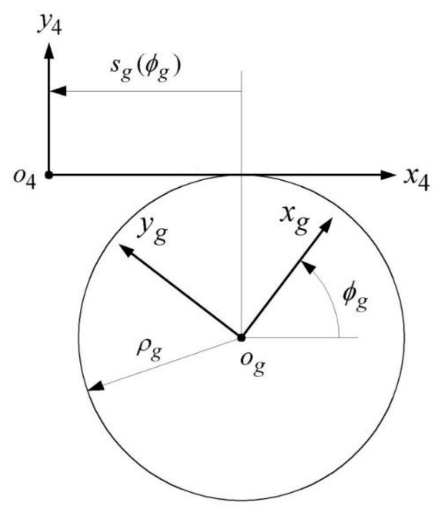

Fig. 8 Relationship between $S_4(x_4,y_4,z_4)$ and $S_g(x_g,y_g,z_g)$.

In the coordinate system $S_g(x_g,y_g,z_g)$, the revolution surface 121 forms a family of surfaces $\{\Sigma_g\}$, the position vector function of which is $\mathbf{r}_g^{(4)}(u_2,\theta_2,\phi_g)$.

$$\mathbf{r}_g^{(4)}(u_2,\theta_2,\phi_g)=\mathbf{M}_{g4}(\phi_g)\mathbf{r}_4(u_2,\theta_2) \tag{16}$$

where

$$\mathbf{M}_{g4}=\begin{bmatrix}\cos\phi_g & \sin\phi_g & 0 & \rho_g(-\phi_g\cos\phi_g+\sin\phi_g)\\ -\sin\phi_g & \cos\phi_g & 0 & \rho_g(\phi_g\sin\phi_g+\cos\phi_g)\\ 0 & 0 & 1 & 0\\ 0 & 0 & 0 & 1\end{bmatrix}$$

The unit normal vector function of the family of surfaces $\{\Sigma_g\}$ is $\mathbf{n}_g^{(4)}(u_2,\theta_2,\phi_g)$.

$$\mathbf{n}_g^{(4)}(u_2,\theta_2,\phi_g)=\mathbf{L}_{g4}(\phi_g)\mathbf{n}_4(u_2,\theta_2) \tag{17}$$

where

$$\mathbf{L}_{g4}(\phi_g)=\begin{bmatrix}\cos\phi_g & \sin\phi_g & 0\\ -\sin\phi_g & \cos\phi_g & 0\\ 0 & 0 & 1\end{bmatrix}$$

The necessary condition for the existence of the envelope of this family of surfaces $\{\Sigma_g\}$ is as follows:

$$f_2(u_2,\theta_2,\phi_g)=\mathbf{n}_4(u_2,\theta_2)\cdot\mathbf{V}_4^{(4g)}(u_2,\phi_g)=0 \tag{18}$$

where

$$\mathbf{V}_4^{(4g)}(u_2,\phi_g)=\begin{bmatrix} y_2\\ \rho_2+\rho_g\phi_g-(x_2+\rho_2)\cos\theta_2\\ 0\end{bmatrix}$$

The mathematical model of the position vector function of the gear 12 can then be represented by

$$\begin{cases}\mathbf{r}_g(u_2,\theta_2,\phi_g)=\mathbf{r}_g^{(4)}(u_2,\theta_2,\phi_g)\\ f_2(u_2,\theta_2,\phi_g)=\mathbf{n}_4(u_2,\theta_2)\cdot\mathbf{V}_4^{(4g)}(u_2,\phi_g)=0\end{cases} \tag{19}$$

The mathematical model of the unit normal vector function of the gear 12 can then be represented by

$$\begin{cases}\mathbf{n}_g(u_2,\theta_2,\phi_g)=\mathbf{n}_g^{(4)}(u_2,\theta_2,\phi_g)\\ f_2(u_2,\theta_2,\phi_g)=\mathbf{n}_4(u_2,\theta_2)\cdot\mathbf{V}_4^{(4g)}(u_2,\phi_g)=0\end{cases} \tag{20}$$

The Method for Generating the Predesigned Fourth-Order Transmission Error

The next step is to accurately design the tooth profile parameters of the pinion, namely C_2, C_3, and C_4, to achieve the predesigned fourth-order transmission error. As illustrated in Figure 9, when the pinion meshes with the gear, the pinion rotates clockwise about the z_p axis with the parameter φ_p, while the gear rotates counterclockwise about the z_g axis with the parameter φ_g. The coordinate system $S_f(x_f, y_f, z_f)$ is a fixed coordinate system rigidly connected to the gearbox. The constraint conditions for any contact point between the pinion and the gear are as follows:

$$\begin{cases} \mathbf{r}_f^{(p)}(u_1,\theta_1,\phi_p,\varphi_p) - \mathbf{r}_f^{(g)}(u_2,\theta_2,\phi_g,\varphi_g) = \mathbf{0} \\ \mathbf{n}_f^{(p)}(u_1,\theta_1,\phi_p,\varphi_p) - \mathbf{n}_f^{(g)}(u_2,\theta_2,\phi_g,\varphi_g) = \mathbf{0} \\ f_1(u_1,\theta_1,\phi_p) = 0 \\ f_2(u_2,\theta_2,\phi_g) = 0 \end{cases} \tag{21}$$

where

$$\begin{cases} \mathbf{r}_f^{(p)}(u_1,\theta_1,\phi_p,\varphi_p) = \mathbf{M}_{fp}(\varphi_p)\mathbf{r}_p(u_1,\theta_1,\phi_p) \\ \mathbf{n}_f^{(p)}(u_1,\theta_1,\phi_p,\varphi_p) = \mathbf{L}_{fp}(\varphi_p)\mathbf{n}_p(u_1,\theta_1,\phi_p) \\ \mathbf{r}_f^{(g)}(u_2,\theta_2,\phi_g,\varphi_g) = \mathbf{M}_{fg}(\varphi_g)\mathbf{r}_g(u_2,\theta_2,\phi_g) \\ \mathbf{n}_f^{(g)}(u_2,\theta_2,\phi_g,\varphi_g) = \mathbf{L}_{fg}(\varphi_g)\mathbf{n}_g(u_2,\theta_2,\phi_p) \end{cases}$$

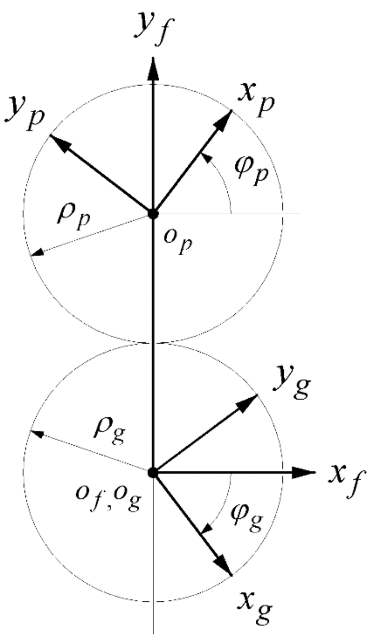

Fig. 9 Relationship between $S_p(x_p, y_p, z_p)$ and $S_g(x_g, y_g, z_g)$.

The pinion and gear rotation angles are φ_p and φ_g, respectively. The transmission error of the gear drive is determined by

$$\Delta\varphi_g = \varphi_g(\varphi_p) - \frac{T_p}{T_g}\varphi_p \tag{22}$$

The slope of the transmission error is determined by

$$\begin{aligned} h_\Delta &= \frac{d(\Delta\varphi_g)}{d\varphi_p} = \frac{d\varphi_g}{d\varphi_p} - \frac{T_p}{T_g} \\ &= \frac{\mathbf{n}_f^{(p)} \cdot \left(\mathbf{e}_f^{(p)} \times \mathbf{R}_f^{(p)}\right)}{\mathbf{n}_f^{(p)} \cdot \left(\mathbf{e}_f^{(g)} \times \mathbf{R}_f^{(g)}\right)} - \frac{T_p}{T_g} \end{aligned} \tag{23}$$

where

$$\mathbf{n}_f^{(p)} = \mathbf{L}_{fp}\mathbf{n}_p, \mathbf{R}_f^{(p)} = \mathbf{L}_{fp}\mathbf{r}_p, \mathbf{R}_f^{(g)} = \mathbf{L}_{fg}\mathbf{r}_g$$
$$\mathbf{e}_f^{(p)} = \{0,0,1\}^T, \mathbf{e}_f^{(g)} = \{0,0,-1\}^T$$

The desired shape of the predesigned fourth-order transmission error is as shown in Fig. 10. Assuming that the pinion and the gear make contact at point R, the following conditions hold:

$$\begin{cases} u_1 = u_{1\mathrm{R}},\ \theta_1 = \theta_{1\mathrm{R}},\ \phi_p = \phi_{pR},\ \phi_g = \phi_{gR}, \\ u_2 = u_{2\mathrm{R}},\ \theta_2 = \theta_{2R},\ \varphi_p = \varphi_{pR},\ \varphi_g = \varphi_{gR} \end{cases} \tag{24}$$

Assuming further that the pinion and the gear make contact at point L, the following conditions hold:

$$\begin{cases} u_1 = u_{1\mathrm{L}},\ \theta_1 = \theta_{1\mathrm{L}},\ \phi_p = \phi_{pL},\ \phi_g = \phi_{gL} \\ u_2 = u_{2\mathrm{L}},\ \theta_2 = \theta_{2L},\ \varphi_p = \varphi_{pL},\ \varphi_g = \varphi_{gL} \end{cases} \tag{25}$$

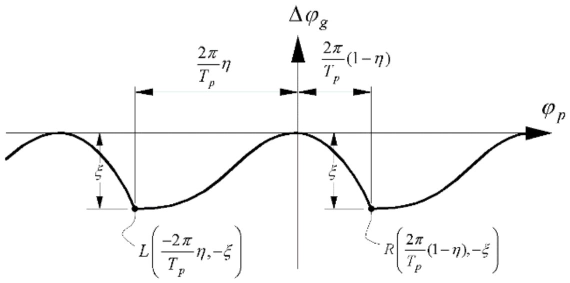

Fig. 10 Desired shape of the predesigned fourth-order transmission error.

At contact point R the following constraint conditions hold:

$$\begin{cases} \mathbf{r}_f^{(p)}(u_{1\mathrm{R}},\theta_{1\mathrm{R}},\phi_{pR},\varphi_{pR}) - \mathbf{r}_f^{(g)}(u_{2\mathrm{R}},\theta_{2\mathrm{R}},\phi_{gR},\varphi_{gR}) = \mathbf{0} \\ \mathbf{n}_f^{(p)}(u_{1\mathrm{R}},\theta_{1\mathrm{R}},\phi_{pR},\varphi_{pR}) - \mathbf{n}_f^{(g)}(u_{2\mathrm{R}},\theta_{2\mathrm{R}},\phi_{gR},\varphi_{gR}) = \mathbf{0} \\ f_1(u_{1R},\theta_{1R},\phi_{pR}) = 0 \\ f_2(u_{2R},\theta_{2R},\phi_{gR}) = 0 \end{cases}$$

(26)

At contact point L, the following constraint conditions hold:

$$\begin{cases} \mathbf{r}_f^{(p)}(u_{1\mathrm{L}},\theta_{1\mathrm{L}},\phi_{pL},\varphi_{pL})-\mathbf{r}_f^{(g)}(u_{2\mathrm{L}},\theta_{2\mathrm{L}},\phi_{gL},\varphi_{gL})=\mathbf{0} \\ \mathbf{n}_f^{(p)}(u_{1\mathrm{L}},\theta_{1\mathrm{L}},\phi_{pL},\varphi_{pL})-\mathbf{n}_f^{(g)}(u_{2\mathrm{L}},\theta_{2\mathrm{L}},\phi_{gL},\varphi_{gL})=\mathbf{0} \\ f_1(u_{1L},\theta_{1L},\phi_{pL})=0 \\ f_2(u_{2L},\theta_{2L},\phi_{gL})=0 \end{cases} \tag{27}$$

At contact point L, there is also a condition where the transmission error slope is zero.

$$h_\Delta(u_{1\mathrm{L}},\theta_{1\mathrm{L}},\phi_{pL},u_{2\mathrm{L}},\theta_{2L},\phi_{gL},\varphi_{pL},\varphi_{gL})=0 \tag{28}$$

According to the desired shape of the predesigned fourth-order transmission error shown in Fig. 10，the values of φ_{pL}, φ_{pR}, φ_{gL}, and φ_{gR} are known as follows:

$$\begin{aligned} &\varphi_{pL}=\frac{-2\pi}{T_p}\eta,\ \varphi_{gL}=-\xi+(T_p/T_g)\varphi_{pL}, \\ &\varphi_{pR}=\varphi_{pL}+\frac{2\pi}{T_p},\ \varphi_{gR}=-\xi+(T_p/T_g)\varphi_{pR} \end{aligned} \tag{29}$$

As $\left|\mathbf{n}_f^{(p)}\right|=\left|\mathbf{n}_f^{(g)}\right|=1$, there are a total of fifteen independent nonlinear algebraic equations, while there are only twelve unknowns: $u_{1\mathrm{L}}$, $\theta_{1\mathrm{L}}$, ϕ_{pL}, $u_{2\mathrm{L}}$, θ_{2L}, ϕ_{gL}, $u_{1\mathrm{R}}$, $\theta_{1\mathrm{R}}$, ϕ_{pR}, $u_{2\mathrm{R}}$, $\theta_{2\mathrm{R}}$, and ϕ_{gR}. The additional three equations can be used to solve for the three undetermined coefficients, C_2, C_3, and C_4, which are the tooth profile parameters of the pinion. In other words, considering the three undetermined coefficients as unknowns, Eqs. (26)-(29) form a system of fifteen nonlinear equations with fifteen unknowns.

$$\begin{aligned} &F_i(\mathbf{X})=0,\ i=1,2,\cdots,15 \\ &\mathbf{X}=\{u_{1L},\ \theta_{1L},\ \phi_{pL},\ u_{2L},\ \theta_{2L},\ \phi_{gL},\ u_{1R},\ \theta_{1R},\ \phi_{pR}, \\ &u_{2R},\ \theta_{2R},\ \phi_{gR},\ C_2,\ C_3,\ C_4\} \end{aligned} \tag{30}$$

In order to solve the roots of the system of nonlinear equations, this study uses the differential evolution algorithm for global search. The convergent results obtained from the search are then passed to the Newton method as initial guesses, and the exact solution of the roots is obtained using the Newton method. Through the above method, the exact design values of the three undetermined coefficients, C_2, C_3, and C_4, can be obtained.

TOOTH CONTACT ANALYSIS

This study presents a numerical example of tooth contact analysis, evaluating the actual transmission error, contact points, contact ellipses, and bearing contacts. The parameter settings used in the example are shown in Table 1, where C_2, C_3, and C_4, are obtained by solving the system of equations in Eq. (30).

Table 1. Parameter settings of the numerical example.

Parameter	Symbol	Value	Unit
Module	m	10	mm
Number of teeth of the pinion 11	T_p	20	--
Number of teeth of the gear 12	T_g	33	--
Radius parameter of the revolution surface 111	ρ_1	90	mm
Radius parameter of the revolution surface 121	ρ_2	108	mm
Dedendum	h_f	$1.25m$	mm
Pitch radius of the pinion 11	ρ_p	$mT_p/2$	mm
Pitch radius of the gear 12	ρ_g	$mT_g/2$	mm
Generating motion parameter	C_2	0.61646	mm/rad^2
Generating motion parameter	C_3	-2.59776	mm/rad^3
Generating motion parameter	C_4	2.48605	mm/rad^4
Range of the predesigned fourth-order transmission error	ξ	10	arcsec
Proportion of the left side of the predesigned fourth-order transmission	η	0.7	--

error			

According to Litvin (1994), solving the following system of nonlinear equations enables the execution of tooth contact analysis. This analysis provides the numerical values of the parameters of the contact points, the coordinates of the contact points, and the actual transmission error values when the pinion and the gear are in actual contact.

$$\begin{cases} \mathbf{r}_f^{(p)}(u_1,\theta_1,\phi_p,\varphi_p)-\mathbf{r}_f^{(g)}(u_2,\theta_2,\phi_g,\varphi_g)=\mathbf{0} \\ \mathbf{n}_f^{(p)}(u_1,\theta_1,\phi_p,\varphi_p)-\mathbf{n}_f^{(g)}(u_2,\theta_2,\phi_g,\varphi_g)=\mathbf{0} \\ f_1(u_1,\theta_1,\phi_p)=0 \\ f_2(u_2,\theta_2,\phi_g)=0 \end{cases} \tag{31}$$

Table 2 presents the relationship between the angle of the pinion and the real transmission error. Fig. 11 illustrates the real motion curve generated by the real transmission error over three cycles.

Table 2. Angle of pinion versus real transmission error.

φ_p Angle of pinion (rad)	$\Delta\varphi_g$ Real transmission error (arcsec)
-0.21991	-10.00000
-0.18425	-9.43400
-0.14859	-7.88678
-0.11293	-5.67348
-0.07727	-3.23029
-0.04160	-1.11813
-0.00594	-0.02684
0.02945	-0.76448
0.06480	-4.24611
0.09425	-10.00000

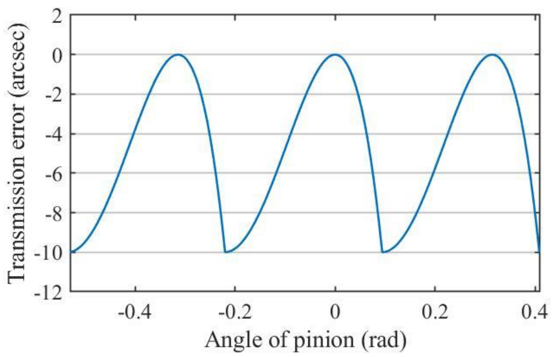

Fig. 11 Real motion curve.

Through polynomial regression analysis, the following regression equation is derived. The R-squared value for this equation is 1, confirming that the real transmission error precisely adheres to a fourth-order polynomial function.

$$\begin{cases} \Delta\varphi_g = a_0 + a_1\varphi_p + a_2\varphi_p^2 + a_3\varphi_p^3 + a_4\varphi_p^4 \\ a_0 = 0.00107286 \\ a_1 = -0.0643894 \\ a_2 = -780.423 \\ a_3 = -3341.15 \\ a_4 = -3339.95 \\ -0.21991 \le \varphi_p \le 0.09425 \end{cases} \tag{32}$$

By substituting the numerical values of the parameters of the contact points into the principal curvatures and directions of the tooth surfaces of both the pinion and the gear, the major and minor axes, as well as the orientation of the contact ellipses, can be determined. Figure 12 illustrates the contact ellipses and bearing contacts on the pinion and gear. It can be observed that the bearing contacts on both the pinion and gear are located in the central region of the tooth surfaces, indicating the absence of edge contact and edge stress concentration issues. In Fig. 13, the application of the multibody dynamics analysis software Recurdyn to simulate the meshing and contact pressure of the gear drive is depicted. The angular velocity applied on the pinion is set to 60 RPM, the torque applied on the gear is set to 5000 N-mm, and the material is set to steel. This analysis allows for checking whether the pinion and gear are in proper contact or if interference occurs where it should not. A video showcasing the entire simulation has been uploaded to the YouTube platform, and the video's URL is https://youtu.be/ujLZIHW5vW4.

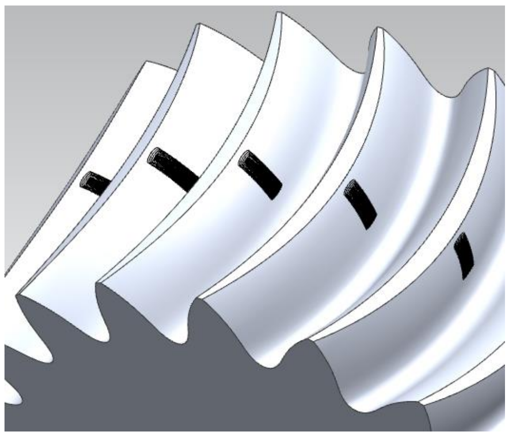

(a)

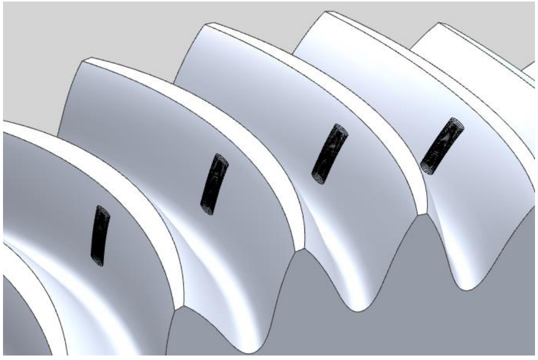

(b)

Fig. 12 Contact ellipses and bearing contacts on the (a) pinion and (b) gear.

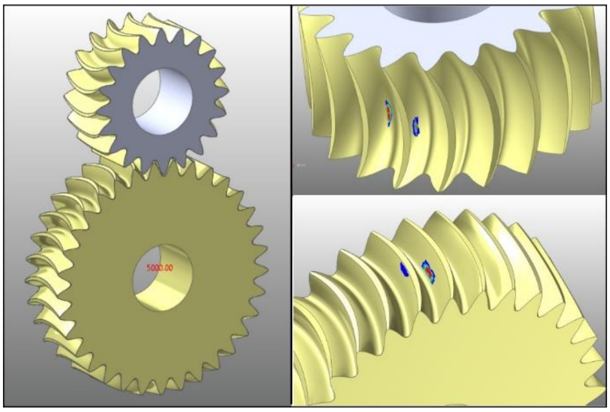

Fig. 13 Meshing and contact pressure simulation.

COMPUTER NUMERICAL CONTROL MACHINING

This study employs a four-axis computer numerical control (CNC) machine for machining the gear drive. Owing to the dimensional limitations of this CNC machine on workpieces, the geometric models are proportionally reduced by one-fourth. Computer-aided design and manufacturing software, Siemens NX, is utilized to generate the CNC program for the machining process. Initially, the toolpath for machining a single tooth space is planned, as illustrated in Fig. 14. Subsequently, the process for a single tooth space is extrapolated to encompass all tooth spaces, as shown in Fig. 15. After obtaining the toolpaths for all tooth spaces, a simulation of all processes is conducted to confirm the correctness of the procedures, as depicted in Fig. 16. Finally, the toolpaths are post-processed to generate the CNC program, as illustrated in Fig. 17.

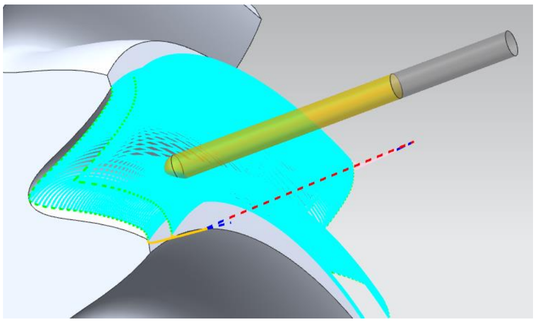

Fig. 14 Toolpath planning for a single tooth space.

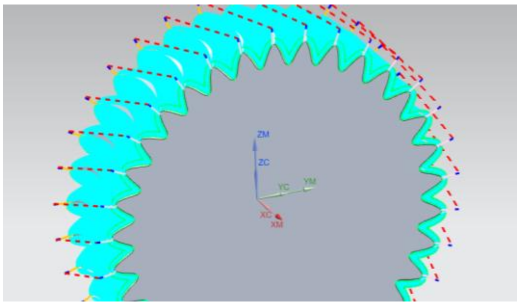

Fig. 15 The result after extending the process of a single tooth space to all tooth spaces.

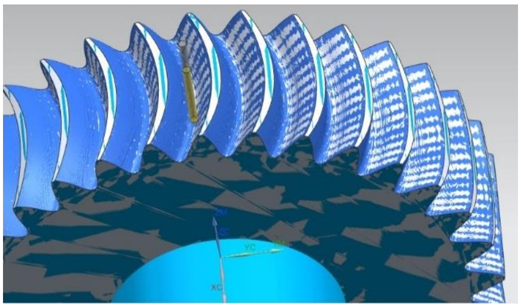

Fig. 16 Simulating all processes to confirm the correctness of the procedures.

```
%
N0010 G40 G17 G90 G71
N0020 G91 G28 Z0.0
N0030 T01 M06
N0040 G00 G90 X-52.085 Y-1.376 A9.372 S3000 M03
N0050 G43 Z193.322 H01
N0060 Z188.322
N0070 G01 Z182.502 F100. M08
N0080 X-52.014 Y-1.329 Z181.855
N0090 X-51.806 Y-1.192 Z181.252
N0100 X-51.475 Y-.973 Z180.734
N0110 X-51.043 Y-.688 Z180.336
N0120 X-50.54 Y-.356 Z180.086
N0130 X-50. Y0.0 Z180.
N0140 X-49.109 A9.185
N0150 X-48.213 A9.002
N0160 X-47.311 A8.822
N0170 X-46.397 Z180.001 A8.644
N0180 X-45.476 A8.469
N0190 X-44.551 A8.298
```

Fig. 17 The CNC program generated by post-processing of toolpaths.

This study also incorporates numerical control machining simulation verification software VERICUT to simulate the entire machining process. Firstly, a complete CNC machine model, including geometric and controller models, must be established in VERICUT. The CNC machine used in this study is a four-axis machine with XYZ translation axes and one A rotational axis. Secondly, geometric models of the machining tool and gear workpiece are created in VERICUT. Finally, by importing the CNC program, the entire machining process can be simulated. As shown in Fig. 18, during the simulation process, the motion of the machine, tool, and workpiece can be clearly observed. VERICUT automatically detects any collisions and issues an immediate alert in case of occurrence. Upon completion of the machining process, an automated comparison analysis is performed to check for issues such as over-cutting or remaining material, as illustrated in Fig. 19.

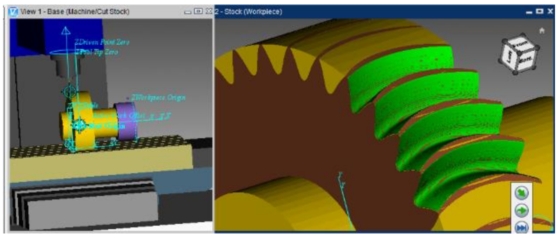

Fig. 18 Using VERICUT software to simulate the entire process of numerical control machining.

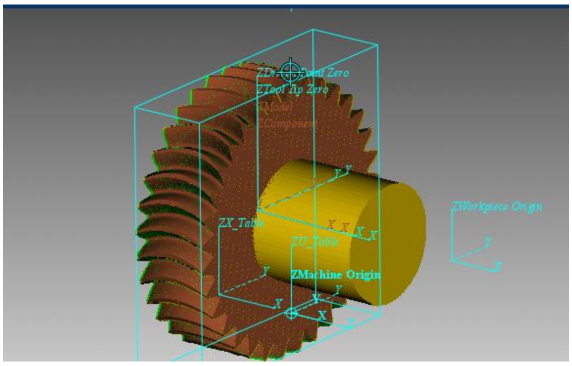

Fig. 19 Utilizing automated comparative analysis to inspect for issues such as over-cutting or remaining material.

After simulating the machining process on the computer and confirming that there are no issues, the final step involves actual gear machining on the real four-axis CNC machine. Figure 20 illustrates the rough machining of the gear workpiece, while Figure 21 shows the finishing process. A video showcasing the entire CNC machining process has been uploaded to the YouTube platform, and the video's URL is https://youtu.be/JuRLsDACgjY. Figure 22 displays the finished pinion and gear. Figure 23 presents using red ink to analyze bearing contacts. The result indicates that the bearing contacts are concentrated in the central regions of tooth surfaces, with no edge contact, consistent with the results of tooth contact analysis.

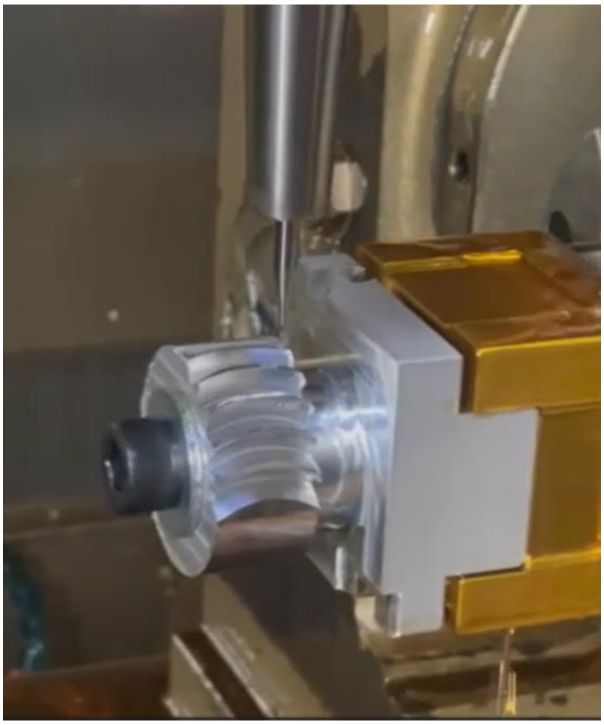

Fig. 20 Conducting rough machining of the workpiece.

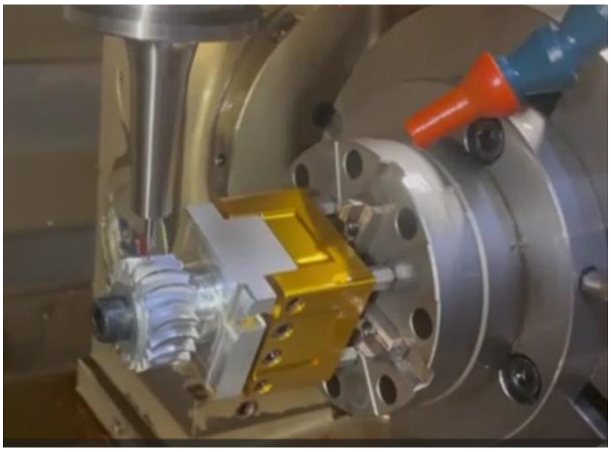

Fig. 21 Conducting precision machining of the workpiece.

Fig. 22 The finished pinion and gear.

Fig. 23 Using red ink to analyze bearing contacts.

CONCLUSIONS

This study has introduced and analyzed a promising curvilinear cylindrical gear drive with a predesigned fourth-order transmission error and cosine tooth profile, offering potential benefits such as smoother operation, compactness, and reduced stress concentration. The research meticulously explored various aspects, including developing mathematical models for both the pinion and gear and implementing a system of constraint equations to achieve the predesigned transmission error. Differential evolution and Newton's method were employed to precisely determine the unknown design parameters. Furthermore, the study validated the actual transmission error and contact patterns through comprehensive tooth contact analysis (TCA) and multibody dynamics simulation. It successfully demonstrated the practical feasibility of machining the gear drive using CAD/CAM and a four-axis CNC machine. Key findings confirmed that the designed gear drive achieved the intended fourth-order transmission error, with bearing contacts strategically located in the central regions of the tooth surfaces. The flawless execution of the CNC machining process showcased the design's manufacturability, and the red ink inspection validated the TCA results, confirming proper bearing contact location. Further research to explore its behavior under various operating conditions and optimize for specific applications has the potential to unlock its full capabilities and significantly contribute to advancing gear technology.

ACKNOWLEDGMENT

Financial support for this work was provided by the National Science and Technology Council in Taiwan, R.O.C, under the contract MOST 111-2637-E-230-007.

REFERENCES

Arafa, H.A., “C-gears: geometry and machining,” *Proceedings of the Institution of Mechanical Engineers, Part C: Journal of Mechanical Engineering Science*, Vol. 219, No. 7, pp. 709-726 (2005).

Chen, Y.C. and Gu, M.L., “Tooth contact analysis of a curvilinear gear set with modified pinion tooth geometry,” *Proceedings of the Institution of Mechanical Engineers, Part C: Journal of Mechanical Engineering Science*, Vol. 225, No. 4, pp. 975-986 (2011).

Chen, Y.C., Li, Z.W., Lo, C.C. and Wang, Z.G., “A Study on the improvement of meshing characteristics of a complementary curvilinear gear set generated by complementary rack cutters,” *Transactions of the Canadian Society for Mechanical Engineering*, Vol. 41, No. 2, pp. 281-291 (2017).

Chen, Y.C. and Lo, C.C., “Contact stress and transmission errors under load of a modified curvilinear gear set based on finite element analysis,” *Proceedings of the Institution of Mechanical Engineers, Part C: Journal of Mechanical Engineering Science*, Vol. 229, No. 2, pp. 191–204 (2015).

De Donno, M. and Litvin, F.L., “Computerized design and generation of worm gear drives with stable bearing contact and low transmission errors,” *ASME Journal of Mechanical Design*, Vol. 121, No. 4, pp. 573-578 (1999).

Fuentes, A., Ruiz-Orzaez, R. and Gonzalez-Perez, I., “Computerized design, simulation of meshing, and finite element analysis of two types of geometry of curvilinear cylindrical gears,“ *Computer Methods in Applied Mechanics and Engineering*, Vol. 272, pp. 321-339 (2014).

Jiang, J. and Fang, Z., “Design and analysis of modified cylindrical gears with a higher-order transmission error,” *Mechanism and Machine Theory*, Vol. 88, pp. 141-152 (2015).

Koga, T., “Method for cutting paired gears having arcuate tooth trace,” *United States Patent* No. 3915060 (1975).

Lee, C.K. and Chen, C.K., “Mathematical models, meshing analysis and transmission design for a robust cylindrical gear set generated by two blade-discs with parabolic cutting edges,” *Proceedings of the Institution of Mechanical Engineers, Part C: Journal of Mechanical Engineering Science*, Vol. 218, No. 12, pp. 1539-1553 (2004).

Lee, C.K., “Manufacturing process for a cylindrical crown gear drive with a controllable fourth order polynomial function of transmission error,” *Journal of Materials Processing Technology*, Vol. 209, No. 1, pp. 3-13 (2009).

Lee, C.K., “A method to design a new face gear drive that has a predesigned fourth order function of transmission errors and dimensionally controllable contact ellipses,” *Journal of the Chinese Society of Mechanical Engineers*, Vol. 39, No. 5, pp. 459-469 (2018).

Lee, C.K., “The mathematical model and a case study of the cosine face gear drive that has a predesigned fourth order function of transmission errors and a localized bearing contact,” *Advances in Mechanical Engineering*, Vol. 11, No. 2, pp. 1-20 (2019).

Litvin, F.L, Zhang, J., Lee, H.T. and Handschuh, R.F., “Transmission errors and bearing contact of spur, helical and spiral bevel gears,” *SAE Transactions*, Vol. 97, pp. 576-586 (1988).

Litvin, F.L., *Gear geometry and applied theory*, PTR Prentice Hall, Englewood Cliffs, New Jersey, USA (1994).

Litvin, F.L. and Kim, D.H., “Computerized design, generation and simulation of meshing of modified involute spur gears with localized bearing contact and reduced level of transmission errors,” *ASME Journal of Mechanical Design*, Vol. 119, No. 1, pp. 96-100 (1997).

Litvin, F.L. and Lu, J., “Computerized design and generation of double circular-arc helical gears with low transmission errors,” *Computer Methods in Applied Mechanics and Engineering*, Vol. 127, No. 1-4, pp. 57-86 (1995).

Litvin, F.L., Argentieri, G., De Donno, M. and Hawkins, M., “Computerized design, generation and simulation of meshing and contact of face worm-gear drives,” *Computer methods in applied mechanics and engineering*, Vol. 189, No. 3, pp. 785-801 (2000).

Liu, S.T., “Curvilinear cylindrical gears,” *Gear Technology*, Vol. 5, pp. 8-12 (1988).

Seol, I.H. and Litvin, F.L., “Computerized design, generation and simulation of meshing and contact of worm-gear drives with improved geometry,” *Computer Methods in Applied Mechanics and Engineering*, Vol. 138, No. 1-4, pp. 73-103 (1996).

Stadtfeld. H.J. and Gaiser, U., “The ultimate motion graph,” *ASME Journal of Mechanical Design*, Vol. 122, No. 3, pp. 317-322 (2000).

Tseng, R.T. and Tsay, C.B., “Mathematical model and undercutting of cylindrical gear with curvilinear shaped teeth,” *Mechanism and Machine Theory*, Vol. 36, No. 11-12, pp. 1189-1202 (2001).

Tseng, R.T and Tsay, C.B., “Contact characteristics of cylindrical gears with curvilinear shaped teeth,” *Mechanism and Machine Theory*, Vol. 39, No. 9, pp. 905-919 (2004).

Tseng, J.T. and Tsay, C.B., “Mathematical model and surface deviation of cylindrical gears with curvilinear shaped teeth cut by a hob cutter,” *ASME Journal of Mechanical Design*, Vol. 127, No. 5, pp. 982-987 (2005).

Tseng, J.T. and Tsay, C.B., “Undercutting and contact characteristics of cylindrical gears with curvilinear shaped teeth generated by hobbing,” *ASME Journal of Mechanical Design*, Vol. 128, No. 3, pp. 634-643 (2006).

Wang, P.Y. and Fong, Z.H., “Fourth-order kinematic synthesis for face-milling spiral bevel gears with modified radial motion (MRM) correction,” *ASME Journal of Mechanical Design*, Vol. 128, No. 2, pp. 457-467 (2006).

Wei, Y., Li, Z., Liu, Y., Guo, R., Yang, D., Luo, L. and Chen, Z., “Geometric contact characteristics and sensitivity analysis of variable hyperbolic circular-arc-tooth-trace cylindrical gear with error theory considered,” *Journal of Northwestern Polytechnical University*, Vol. 40, No. 3, pp. 679-689 (2022).

Wu, Y., Luo, P., Bai, Q., Liang, S., Fan, Q. and Hou, L. “Modelling and analyzing of loaded meshing characteristics of cylindrical gear transmission with curvilinear-shaped teeth,” *Meccanica*, Vol. 58, No. 8, pp. 1555-1580 (2023).

Wu, Y.C., Chen, K.Y., Tsay, C.B. and Ariga, Y., “Contact characteristics of circular-arc curvilinear tooth gear drives,” *ASME Journal of Mechanical Design*, Vol. 131, No. 8, 081003 (2009).

Zhang, X. and Liang, Z., “Mathematical model and contact characteristics of curvilinear cylindrical gears with line contact,” *Journal of the Brazilian Society of Mechanical Sciences and Engineering*, Vol. 43, Article No. 183 (2021).

Zhang, X., Xie, Y. and Tan, X., “Design, meshing characteristics and stress analysis of cylindrical gears with curvilinear tooth profile," *Transactions of FAMENA*, Vol. 40, No. 1, pp. 27-44 (2016).

NOMENCLATURE

1 the curvilinear cylindrical gear drive

11 the curvilinear cylindrical pinion

111 the revolution surface for the generation of 11

1111 the axial section shape of 111

12 the curvilinear cylindrical gear

121 the revolution surface for the generation of 12

1211 the axial section shape of 121

A_1 the revolution axis of 111

A_2 the revolution axis of 121

C_2, C_3, C_4 the generation motion parameters

h_Δ the slope of the transmission error

$\mathbf{L}_{ij}$ the coordinate transformation matrix of unit normal vector from S_j to S_i

$\mathbf{M}_{ij}$ the coordinate transformation matrix of position vector from S_j to S_i

m the module of the gear drive

$\mathbf{N}_3(u_1,\theta_1)$ the normal vector function of 111

$\mathbf{N}_4(u_2,\theta_2)$ the normal vector function of 121

$\mathbf{n}_3(u_1,\theta_1)$ the unit normal vector function of 111

$\mathbf{n}_4(u_2,\theta_2)$ the unit normal vector function of 121

$\mathbf{n}_p^{(3)}(u_1,\theta_1,\phi_p)$ the unit normal vector function of $\{\Sigma_p\}$

$\mathbf{n}_g^{(4)}(u_2,\theta_2,\phi_g)$ the unit normal vector function of $\{\Sigma_g\}$

$\mathbf{r}_1(u_1)$ the position vector function of 1111

$\mathbf{r}_2(u_2)$ the position vector function of 1211

$\mathbf{r}_3(u_1,\theta_1)$ the position vector function of 111

$\mathbf{r}_4(u_2,\theta_2)$ the position vector function of 121

$\mathbf{r}_p^{(3)}(u_1,\theta_1,\phi_p)$ the position vector function of $\{\Sigma_p\}$

$\mathbf{r}_g^{(4)}(u_2,\theta_2,\phi_g)$ the position vector function of $\{\Sigma_g\}$

T_p the number of teeth of 11

T_g the number of teeth of 12

$\mathbf{X}$ the fifteen unknows to be determined

$\Delta\varphi_g$ the transmission error of the gear drive

η the proportion of the left side of the predesigned fourth-order transmission error

ξ the range of the predesigned fourth-order transmission error

ρ_1 the radius parameter of 111

ρ_2 the radius parameter of 121

ρ_p the pitch radius of 11

ρ_g the pitch radius of 12

$\{\Sigma_p\}$ the family of surfaces formed by 111

$\{\Sigma_g\}$ the family of surfaces formed by 121

具預設四階傳動誤差及餘弦齒形的曲線齒圓柱齒輪傳動之創成、建模與分析

李政鋼
正修科技大學工業工程與管理系
鄭永長
國立高雄科技大學機電工程系

摘 要

本研究提出了一種創新的曲線齒圓柱齒輪傳動，其特點是具預設之四階傳動誤差和餘弦齒形。預設之四階傳動誤差不僅可以吸收線性傳動誤差，還能使整體的運動曲線更加平滑；而餘弦齒形則有助於降低無根切現象發生的最小齒數。研究首先建立了曲線齒小齒輪和大齒輪的創成方法及數學模式。接著依據齒面接觸條件與具預設四階傳動誤差條件建立了一組有十五個未知數與十五個方程式的非線性聯立方程組。之後應用差分進化算法與牛頓法對未知數進行全域搜索與局部精煉以便求得創成運動參數的精確設計解。然後應用齒面接觸分析（TCA）理論驗證了真實傳動誤差與預設之四階傳動誤差完全相符，同時也驗證了接觸橢圓和承壓接觸位於齒面中央部位。最後，為進一步確認理論分析結果的正確性，再應用 CAD/CAM 技術和四軸電腦數值控制工具機製作一組曲線齒圓柱齒輪傳動，經過紅丹檢查承壓接觸位置後，確認真實接觸情形與理論分析的結果相符。